TURBULENT HEAT TRANSFER BETWEEN CONCENTRIC ROTATING CYLINDERS

M. S. Mohamed
Mechanical Power Engineering Department,
Faculty of Engineering, Mansoura University.

إنْتِقَالُ الحَرَارَةِ المُضْطَرِبِ بَيْنَ إسْطُوَانَتَيْنِ دَوَّارَتَيْنِ مُتَحِدَتَيْ المَرْكَزْ.

الخلاصـــة:

فى هذا البحث تم عمل برنامج حاسب للتنبؤ بتأثير دوران الاسطوانة الداخلية والخارجية على شكل السريان وتوزيع درجات الحرارة وانتقال الحرارة فى المسافة الفاصلة بين اسطوانتين متحدتى المركز. فى البحث الحالى استُخْدِمَ نموذج اضطراب ذو معادلتين بعد تعديله لكى يأخذ فى الإعتبار تأثير القوة الطاردة المركزية الناتجة عن دوران الاسطوانتين على زيادة نسبة الاضطراب. ثلاثة نسب للأقطار (هى ٠,٥ ، ٠,٧٥ ، ٠,٨٥٧٥) تم استِخْدامها فى هذه الدراسة . كما تم استِخْدام عدد من سرعات الدوران المختلفة عند سرعات سريان مختلفة فى حالة دوران الاسطوانتين فى اتجاه واحد وفى اتجاهين متضادين. أوضحت المقارنة بين النتائج الحالية والنتائج المعملية المتاحة اتفاقا تاما مما يدل على دقة البرنامج الحالى لحل معادلات الحركة وكذلك دقة التعديلات التى أُدْخِلَتْ على نموذج الاضطراب.

ABSTRACT:

A finite-difference technique is developed to predict the effect of rotation of the inner and outer cylinders on the turbulent fluid flow and heat transfer in concentric rotating cylinders. In the present investigation the two-equation model of turbulence (k-ε) is employed. The constants of the model are adjusted to take into account the express increase or suppression of turbulence due to the centrifugal force in the fluid caused by the cylinders rotation.

The numerical computations are carried out for the radii ratios 0.5, 0.75 and 0.8575. Different tangential velocity ratios at different axial Reynolds numbers, for co-rotating and counter rotating cylinders, were investigated. The present numerical predictions are compared with the available data [17]. The comparison showed excellent agreement that confirms the accuracy of the present numerical algorithm together with the turbulence model modifications.

1. INTRODUCTION

Fluid flow and heat transfer between concentric rotating cylinders have been of great interest for many years. It has many engineering applications such as turbomachinary, rotating electric machines, swirl nozzles, combustion chambers and fusion reactors. So, it has been subjected to many analytical and experimental investigations.

Several studies [1-4] have been carried out on fluid flow and heat transfer in an annulus for the simplest case of axial flow with no boundary rotation. The investigation of Malik and Pletcher [4] is the most comprehensive prediction of the non-rotating straight annulus flow with heat transfer. Some others [5-7] have studied the case of either cylinder rotation with no axial flow. They established the various flow modes in the annulus as well as their stability conditions as a function of the modified Taylor number. Four flow regimes were recognized: laminar, laminar with Taylor vortices, turbulent with Taylor vortices and a fully turbulent regime.

Luck [8] was the first to investigate the mixed mode case of axial flow with the inner cylinder rotating. Such flow occurs in the cooling of electrical motors. This was later extended for different gap ratios by Gasley [9], and Becker and Kaye [10]. Tachinbana and Fukui [11] suggested a correlation for Nusselt number for the narrow annulus gap taking into account thermal entrance effects. Molozhen and Polyak [12] offered a heat transfer correlation for the two limiting cases of axial flow with no rotation, and rotating inner cylinder with no axial flow. Kuzay and Scott [13] carried out experimental measurements of the heat transfer rate in a large gap annulus with inner

Accepted March 24, 1998

cylinder rotation. They measured both the axial and radial temperature distributions, and proposed a correlation for Nusselt number as a function of the ratio of axial travel of the flow helix in terms of hydraulic diameter per half revolution of the spinning wall.

Abou-Ellail and Morcos [14] predicted numerically the turbulent flow field and heat transfer in the entrance region of an annulus with both rotating inner cylinder and non-rotating one. The outer cylinder was uniformly heated while the inner one was taken to be thermally insulated. They compared their results with the experimental results of previous investigator. The comparison showed good agreement over the entire rage of the parameters considered. Some deviations between experimental and theoretical data are, however, noticed in the case of high rotational speeds. They also adjusted the constants of the two-equations model of turbulence (k-ε model) [15] to account for the rotation of the inner cylinder by decreasing the dissipation rate of the kinetic energy of turbulence. In this way the level of turbulence is greatly enhanced with inner cylinder rotation.

The stability of circular Coutte flow with radial heating across a vertically oriented annulus with inner cylinder rotating and outer cylinder stationary is investigated by Ali and Weidman [16]. They used a linear stability theory. The numerical investigation is restricted to radius ratios of 0.6 and 0.959 at Prandtl number 4.35, 15 and 100. The results follow the development of critical stability from Taylor cells at zero heating through a number of asymmetric modes to axisymmetric cellular convection at zero rotation. Increasing the Prandtl number profoundly destabilizes the flow in both wide and narrow gaps and the number of contending critical modes increases with increasing radius ratio. Some of their results
were compared with the stability measurements of other investigators and they have got good agreement.

Pfitzer and Beer [17] were the first to examine (theoretically and experimentally) the heat transfer of turbulent axial flow in an annulus with co-rotating and counter-rotating tubes. In the experimental investigation, the heat transfer rate in the hydrodynamic and thermal entrance regions of the rotating annulus and the velocity and temperature profiles at the end of the test section were determined. The analytical study was performed for flow and heat transfer of fully developed flow in a rotating annulus by applying a modified mixing length theory. The theoretical results for fully developed flow are compared with the experimental data at the axial position of 60 hydraulic diameters downstream of the entrance.

This paper describes the effect of independently rotating inner and outer cylinders of a concentric annulus on the velocity, turbulence intensity, shear stress and temperature distribution and on the heat transfer to the air which is flowing inside the annular gap. The two-equation model of turbulence the k-ε model is employed in this investigation. Modifications that take into account the effect of rotation of one or the two cylinders were implemented into the original model.

2. GOVERNING EQUATIONS

Assume that the fluid has constant physical properties and the flow is steady axisymmetric with the absence of body forces. Applying the well known Prandtl boundary layer assumptions and checking the order of magnitude of each term of the boundary layer equations [18]: the equations governing the fluid motion in an annulus with rotating cylinders and axial throughflow, in the entry region, may be reduced to the following simplified boundary layer equations:

Continuity equation:

$$\frac{\partial (r V_z)}{\partial z} + \frac{\partial (r V_r)}{\partial r} = 0 \qquad \text{..... (1)}$$

r-momentum equation:

$$\rho \frac{V_\theta^2}{r} = \frac{\partial P}{\partial r} \qquad \text{..... (2)}$$

θ-momentum equation:

$$V_r \frac{\partial V_\theta}{\partial r} + V_z \frac{\partial V_\theta}{\partial z} = \frac{\nu}{r} \frac{\partial}{\partial r} \left(r \frac{\partial V_\theta}{\partial r} \right) \qquad \text{.....(3)}$$

z -momentum equation:

$$V_r \frac{\partial V_z}{\partial r} + V_z \frac{\partial V_z}{\partial z} = -\frac{1}{\rho}\frac{\partial P}{\partial z} + \nu\left[\frac{1}{r}\frac{\partial}{\partial r}\left(r\frac{\partial V_z}{\partial r}\right) + \frac{\partial^2 V_z}{\partial z^2}\right] \quad \text{..... (4)}$$

Energy equation:

$$\rho c_p V_z \frac{\partial T}{\partial z} = -\frac{1}{r}\frac{\partial}{\partial r}\left(r\dot{q}_r\right) \quad \text{..... (5)}$$

The radial component of the heat flux vector is

$$\dot{q}_r = -\lambda\frac{\partial T}{\partial r} + \rho c_p \overline{v'_r T'} \quad \text{..... (6)}$$

where T is the average temperature, T' is temperature fluctuations, c_p is the specific heat at constant pressure and λ is the thermal conductivity.

Scalar property ϕ:

The transport equation of the scalar quantities: turbulent kinetic energy k, turbulence dissipation rate ε and the Reynolds stresses in a general from is:

$$\rho\frac{\partial}{\partial z}\left(rV_z\phi\right) + \rho\frac{\partial}{\partial r}\left(rV_r\phi\right) = -\frac{\partial}{\partial r}\left(rJ_r\phi\right) + P_\phi - D_\phi \quad \text{..... (7)}$$

where ϕ is the required scalar quantity. J_ϕ is the flux of the scalar property ϕ, P_ϕ is the production rate of ϕ and D_ϕ is the dissipation rate of ϕ. The velocity components (V_z, V_r and V_θ) and the scalar property ϕ represent time average values.

The fully developed flow, which establishes if the annulus is sufficiently long, provides good analytical check on the finite difference solution to be obtained. The equations of conservation for an incompressible turbulent fully developed flow will take the form.

$$V_r = 0 \quad \text{..... (8)}$$

$$\rho\frac{V_\theta^2}{r} = \frac{\partial P}{\partial r} \quad \text{..... (9)}$$

$$0 = \frac{2}{r}\tau_{r\theta} + \frac{\partial \tau_{r\theta}}{\partial r} \quad \text{..... (10)}$$

$$0 = -\frac{\partial P}{\partial z} + \frac{\partial \tau_{rz}}{\partial r} + \frac{\tau_{rz}}{r} \quad \text{..... (11)}$$

For a Newtonian fluid with constant physical properties, the components of the stress tensor can be written as:

$$\tau_{r\theta} = \mu\left[r\frac{\partial}{\partial r}\left(\frac{V_\theta}{r}\right)\right] - \rho\overline{v_r v_\theta} \qquad \text{and} \qquad \tau_{rz} = \mu_l\frac{\partial V_z}{\partial r} - \rho\overline{v_z v_r}$$

Because of the assumption of a fluid with constant properties, the equations of motion and energy balance are uncoupled and will be solved separately.

3. TURBULENCE MODEL

The statistical correlations involving the fluctuating velocities and temperatures (e.g. $\overline{u_i u_j}$ and $\overline{u_i T}$), that appear in the momentum and energy equations as a result of the time averaging process, have to be modeled in terms of other known mean quantities. In this investigation, an eddy viscosity model (k-ε) has been employed to calculate these correlations. The k-ε model is a two-equation model of turbulence. For constant (unit) density flow, this model relates the Reynolds stress and heat flux to the mean velocity and temperature gradients as follow

$$\overline{u_i u_j} = \frac{2}{3}\delta_{ij} k - 2\upsilon_t S_{ij} \qquad \text{..... (12)}$$

and

$$-\rho c_p \overline{u_i T} = \lambda_t \frac{\partial T}{\partial x_i} \qquad \text{..... (13)}$$

and in particular

$$-\overline{v_r v_z} = \upsilon_t \frac{\partial V_z}{\partial r} \quad \text{and} \quad -\overline{v_r v_\theta} = \upsilon_t r \frac{\partial}{\partial r}\left(\frac{V_\theta}{r}\right) \qquad \text{..... (14)}$$

where

δ_{ij} is the KRONECKER delta and S_{ij} = mean strain = $\frac{1}{2}\left[\frac{\partial U_i}{\partial x_j} + \frac{\partial U_j}{\partial x_i}\right]$

λ_t is the eddy conductivity which can be related to μ_t by defining a turbulent Prandtl number σ_t such as:

$$\sigma_t = \frac{\mu_t C_p}{\lambda_t} \qquad \text{..... (15)}$$

In the present work σ_t was assumed to be constant and equals 0.9. Equation (14) does not allow for a counter gradient diffusion and more elaborate models are usually required to model the scalar fluxes in this equation [19]. Swirl, buoyancy and transverse streamline curvature [20] affect considerably the turbulence structure causing the heat transfer and skin friction to be different from those predicted by the usual eddy viscosity models. However, since the present work does not emphasize a comparative study for the validity of different turbulence models, the k-ε model will serve as a good tool in predicting the flow in annular geometries, with reasonable accuracy.

The eddy viscosity υ_t can be related to the turbulent structure of the flow by the Prandtl-Kolmogrov relationship [21-22] as follows:-

$$\upsilon_t = C_\mu \left(k^2/\varepsilon\right) \qquad \text{..... (16)}$$

where C_μ is a constant, k is the turbulent kinetic energy ($1/2\ u_i^2$) and ε is the dissipation rate of K $\left(\varepsilon = \upsilon_t \left[\partial\overline{u_i}/\partial\overline{x_j}\right]\right)$.

The turbulence viscosity ν_t is obtained from the solution of the transport equations of k and ε which are determined, in cylindrical polar coordinates, as follows [23] :-

$$\frac{Dk}{Dt} = T_k + P_k - \varepsilon \qquad \text{.....(17)}$$

and

$$\frac{D\varepsilon}{Dt} = T_\varepsilon + \frac{\varepsilon}{k}\left[C_{\varepsilon 1} P_k - C_{\varepsilon 2}\varepsilon\right] \qquad \text{..... (18)}$$

where

P_k = Production rate of k = $\upsilon_t \left[\left(\frac{\partial V_z}{\partial r} \right)^2 + 2 \left(\frac{\partial V_r}{\partial r} \right)^2 + \left(\frac{V_r}{r} \right)^2 \right]$

T_k = Diffusion rate of k = $\frac{1}{r} \frac{\partial}{\partial r} \left[r \left(\nu_l + \frac{\nu_t}{\sigma_{k,t}} \right) \frac{\partial k}{\partial r} \right]$

T_ε = Diffusion rate of ε = $\frac{1}{r} \frac{\partial}{\partial r} \left[r \left(\nu_l + \frac{\nu_t}{\sigma_{\varepsilon,t}} \right) \frac{\partial \varepsilon}{\partial r} \right]$

The empirical coefficients widely used in the standard k-ε model have the following values [24, 25]:

$$C_\mu = 0.09,\ C_{\varepsilon 1} = 1.44,\ C_{\varepsilon 2} = 1.92,\ \sigma_t = 0.9,\ \sigma_{k,t} = 1.0 \text{ and } \sigma_{\varepsilon,t} = 1.3$$

with these values, the wall boundary layers and the plane jet flow are well predicted.

3.1. Initial and Boundary Conditions:

Uniform axial velocity and temperature profiles are assumed at the inlet of the annulus and are equated to the inlet mean values. The radial and tangential velocity profiles are assumed to be zero. The initial distribution of turbulent kinetic energy k and its dissipation rate ε are assumed be to uniform and equal to that values given by Launder and Spalding [26] for turbulent pipe flows. All velocity components along the inner and outer radii are assumed to be zero, expect for the tangential mean velocity at the wall of the inner and outer cylinders. For an annulus having an inner cylinder of radius r_1 and rotates with angular velocity ω_1 while its outer cylinder is of radius r_2 and rotates with angular velocity ω_2, the flow is subjected to the following boundary conditions:

at inlet section ($z=0$)

at $r_1 < r < r_2$

$V_z = \overline{V_z}$ and $T = T_0$ (flat profiles at entrance), $P = P_0 = - V_z^2 / 2$,

$k = 0.003\ V_z^2$ and $\varepsilon = C_\mu k^{3/2} / (0.03\ r_h)$

at the walls $z \geq 0$

at $r = r_1$ $\quad V_r = V_z = 0$ and $V_\theta = \omega_1 r_1$

at $r = r_2$ $\quad V_r = V_z = 0$ and $V_\theta = \omega_1 r_2$

fully developed flow

$\partial / \partial z = 0$ $\quad$ except ($\partial P / \partial z \neq 0$ and $\partial T / \partial z \neq 0$)

The inner cylinder was assumed to be thermally insulated. Therefore, the stagnation enthalpy along the inner cylinder wall is:

$$\left(\partial h / \partial r \right)_{r = r_1} = 0$$

3.2. Near Wall Treatment :

The k-ε is valid only in high Reynolds number flows far form the viscous flow near the wall. Therefore, special treatment is needed to take into account the effect of fluid viscosity on turbulence, particularly, wall shear stress τ_w, wall heat flux q_w, the production of turbulence energy k and its dissipation ε near the wall.

The wall shear stress and wall heat flux were obtained from [26] as:

$$\tau_w = \rho \kappa C_\mu^{1/4} k_P^{1/2} \left| (V_\theta)_w - (V_\theta)_P \right| / \ln (E\ r_P^+) \quad \ldots\ldots\ldots\ldots (19)$$

$$r_P^+ = \rho\ r_P\ C_\mu^{1/4}\ k_P^{1/2} / \mu \quad \ldots\ldots\ldots\ldots (20)$$

$$q_w = \rho C_p (h_w - h_p) C_\mu^{1/4} \kappa_p^{1/2} / \left[\left(\frac{1}{\kappa} ln(E r_p^+) + f_s \right) \sigma_t \right] \quad \text{..... (21)}$$

$$f_s = 9.25 \left(\frac{P_r}{\sigma_t} - 1 \right) \left(\frac{\sigma_t}{P_t} \right)^{0.25}$$

where $\kappa = 0.42$ (Von Karman constant), $E = 9.0$ for smooth walls and P_r is Prandtl number. Subscripts p and w denotes the node p and the wall conditions respectively. In equation (19), the quantity $[(V_0)_w - V_0)_p]$ is employed to account for the rotation of walls.

The production of turbulence near the wall, P_k', can be obtained from the transport equation of k. It was modified in order to take into account the effect of wall shear stress τ_w. It takes the form [23]:

$$P_k' = \tau_w^{3/2} / \rho^{3/2} \kappa r_p \quad \text{..... (22)}$$

The dissipation rate near the wall, ε', was obtained from the assumption that the length scale of turbulence is $L = k^{3/2}/\varepsilon$ which is related to the mixing length as $L = C_\mu^{3/4} \kappa r_p$, thus

$$\varepsilon' = C_\mu^{3/4} k_p^{3/2} / \kappa r_p \quad \text{..... (23)}$$

4. SOLUTION PROCEDURE

The partial differential equations are integrated over a small control volume of the solution domain covering the numerical mesh. This approach leads to intigro-differential equations (finite difference equations) [21].

These can be approximated with the aid of discrete property values located at the grid nodes surrounding the finite volume. The procedure leads to a scheme that reflects the conservation of the fluid property in question. The finite difference equations can be solved on a digital computer. A forward marching procedure is used, in which the properties of the fluid downstream are assumed to be influenced by the conditions upstream only. This procedure is economical because the computer storage required is for two mesh lines only and it is independent of the number of forward steps. Since the procedure has been described in details in reference [20], brief discretion of the method will be mentioned here.

The solution procedure can be summarized in the following steps:

1) After taking a forward step Δx,
2) The V_z velocity field is obtained from the solution of the V_z-momentum equation using the upstream conditions.
3) The V_0 velocity field is obtained from the solution of the V_0-momentum equation .
4) The k, ε and T fields are obtained in sequence form the solution of the respective equations.

In the above finite-difference solution procedure, the two problems of determining the pressure distribution and satisfying the continuity of mass flow are overcome by adjusting the pressure field so as to satisfy continuity. Since the finite-difference equations are non-linear, the above calculation steps are repeated few times before marching downstream to the next cross-stream plane, until the error in each difference equation is less than 0.3%.

5. RESULTS AND DISCUSSION

In all test runs, the numerical computations are curried out for an upward air flow. An axial flow at $Re_z = 10^4$ for a total length $z/D_h = 60$ in an annulus of radius ratio of 0.8575 is used to make comparison between the predicted results and the experimental data of Pfitzer and Beer [17]. Another radii ratio of 0.5 and 0.75 are also employed in the present work. A uniform heat flux from the outer boundary to the fluid flowing through the annulus is imposed.

A non-uniform grid is employed in the radial direction while a constant forward step in the axial direction is used. For the flow field under consideration, a grid of 20 nodes in the radial direction

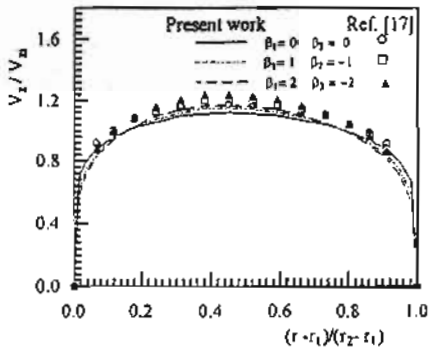

Figure (1) Axial mean velocity at $z/D_h = 60$ and $Re_z = 10^4$

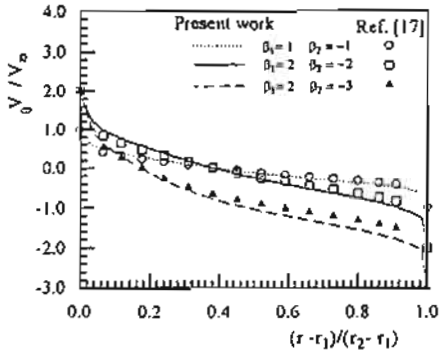

Figure (2) Radial distribution of the tangential mean velocity at $z/D_h = 60$ and $Re_z = 10^4$

and a forward step of (0.01 R_h) in the axial direction was found to give a grid independent solution.

The effect of rotation on heat transfer and fluid flow was studied in the counter-rotating and co-rotating cylinders for different gap ratios $M = r_1/r_2$ at various axial Reynolds numbers Re_z and rotation rates $\beta = V_0 / V_{zi}$. The results are discussed in the following sections:

5.1. Velocity and Temperature Distribution:

Figures (1) through (4) represent the comparison between the case of counter-rotating cylinders ($\zeta = V_{\theta 1}/V_{\theta 2} = -1$) at different rotation ratios (β) and the stationary cylinders ($\zeta = 0$).

Figure (1) shows the comparison between the predicted radial distribution of the axial mean velocity V_z at $z/D_h = 60$ and the experimental data of Pfitzer and Beer [17]. Figure (2) represents the comparison between the predicted radial distribution of the tangential mean velocity V_0 and the available data [17]. Counter-rotating cylinders at tangential velocity ratios $\zeta = V_{\theta 1}/V_{\theta 2} = 0$, -1 and -1.5 are investigated. The two figures are normalized with the entrance axial mean velocity V_{zi}. The comparison indicated that the profiles in both figures approach a more turbulent shape with increasing ζ which is caused by the increase of turbulent fluctuations in the fluid.

Figure (3) represents the comparison between the computed radial temperature Θ distribution and the experimental data [17] for the above cases. The numerical data indicated that large decrease in the wall temperature at the outer rotating cylinder is observed rather than that for non-rotating cylinder $\beta_2 = 0$. The figure indicated that the more increase of the rotation speed β, the more

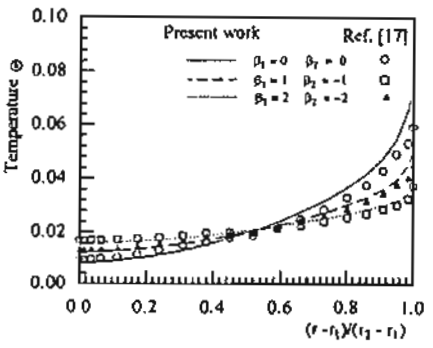

Figure (3) Fluid radial temperature distribution at $z/D_h = 60$ and $Re_z = 10^4$

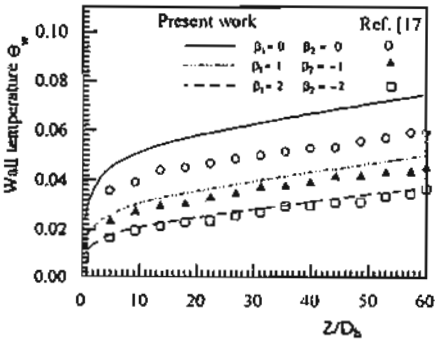

Figure (4) Axial outer wall temperature for $Re_z = 10^4$ at different counter-rotating speed ratios.

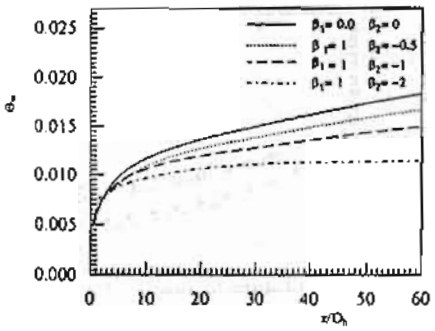

Figure (5) Axial variation of wall temperature for $Re_z = 2.65x\ 10^4$ at different counter-rotating speed ratios.

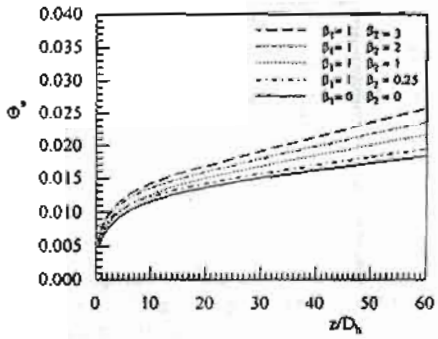

Figure (6) Axial variation of wall temperature for $Re_z = 2.65x\ 10^4$ at different co-rotating speed ratios.

increase of the inner wall temperature while the temperature of the outer cylinder decreases. These changes in the radial temperature distribution can be attributed to the enhanced mixing due to flow rotation between the counter rotating cylinders. The comparison between the theoretical and the experimental data [17] shows that the discrepancy between these curves diminishes with the decrease of the rotational ratios β.

The axial variation of the dimensionless wall temperature Θ_w for counter-rotating cylinders is represented in figures (4). It shows the case of counter-rotating cylinder at $Re_z = 10^4$ at different rotation rates, $\beta = V_\theta/V_{zi}$. At the initial region, z/D_h =10, the figure shows a parabolic increase in the wall temperature, while it attains a linear rise in the fully developed region. The results indicated that increasing the rotation rates β, for the same counter-rotating tangential velocity ratio (ζ = -1), decreases the wall temperature. The figure shows large discrepancy between the predicted and the experimental data [17] for stationary cylinders but this discrepancy diminishes with increasing the rotational ratio β.

The effect of variation of the tangential velocity ratio ζ on the axial wall temperature Θ_w for counter-rotating cylinders is shown in figure (5). The figure represents the comparison of the predicted data for stationary cylinder (ζ = 0) and counter-rotating cylinders at (ζ= -0.5, -1 and -2) for an axial flow of $Re_z = 2.65 \times 10^4$. The figure shows that with rotation, the wall temperature drops below that for the pure axial

case and that the decrease of the wall temperature Θ_w increases with increasing the absolute value of the tangential velocity ratio ζ. The rotating profiles deviates form the non-rotating curves at z/D_h= 5 and this deviation stars faster with increasing the rotation rate. This behaviour can be attributed to the increase of mixing due to flow rotation.

It should be mentioned that co-rotating cylinders has a quite different effect on the temperature profiles. Figure (6) shows the case of co-rotating cylinders of radius ratio 0.75 at $Re_z = 2.65 \times 10^4$. Different tangential velocity ratios (ζ = 0.0, 0.33, 0.5, 1, and 4) were used to indicate the effect of changing the co-rotating tangential velocity ratio (ζ) on the wall temperature. The figure shows that with rotation, the wall temperature gets higher than for the pure axial case. The increase in the wall temperature increases with decreasing the tangential velocity ratio (ζ).

Figure (7) shows the effect of axial Reynolds number and the tangential velocity ratio on the wall temperature. The figure shows the comparison between wall temperature for two pure axial flow (ζ =0) at $Re_z = 2.65 \times 10^4$ and 3.97×10^4 and those rotating profiles for tangential velocity ratio (ζ = -1) at the same two Reynolds number. The figure indicated that the deviation between the rotating and non-rotating curves diminishes with the increase of the axial Reynolds number which is caused by the increase of turbulence intensity in the fluid.

Figure (8) shows the radial temperature profiles for counter-rotating cylinders (ζ =-1.0) at

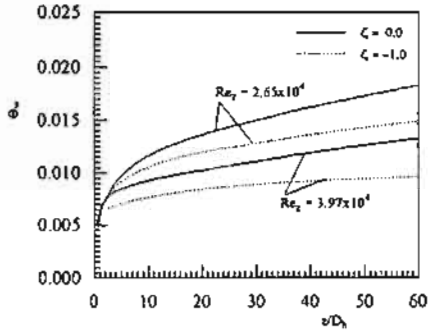

Figure (7) Effect of axial Reynolds number and speed of rotation on the axial wall temperature

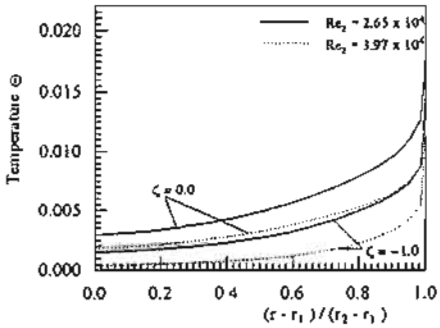

Figure (8) Effect of axial Reynolds number and speed of rotation on the radial temperature distribution at z/D_h =60.

$Re_z = 2.65x10^4$ and $Re_z = 3.97 \times 10^4$ at $z/D_h = 60$. Comparison between the stationary and rotating cylinders is shown. The figure indicated that increasing the axial Reynolds number, for the same co-rotating speed ratio, decreases the dimensionless wall temperature Θ_w for both the inner and outer cylinders.

5.2 Nusselt number:

Figure (9) represents the comparison between the predicted Nusselt number in the present investigation and the experimental data [17]. Figure (9-a) shows the variation of Nusselt number with the axial Reynolds number of the case of inner cylinder rotating while the outer cylinder is stationary. Two rotational Reynolds numbers were investigated $(Re)_{\theta 1} = 10^4$ and $2x10^4$. The figure indicated that with growing the rotational Reynolds number of the inner cylinder $(Re)_{\theta 1}$, while outer cylinder is stationary $(Re)_{\theta 2} = 0$, a remarkable increase in Nusselt number can be observed which is proportional to the rotation rate (β_1). In figure (9-b), the case of outer cylinder rotating while the inner cylinder is stationary has been investigated. The Nusselt number does not change significantly, except for very low flow rate Reynolds number Re_z and high rotation rates β_2. The comparison between the theoretical and experimental data indicated good agreement for the case of stationary cylinders except for very low axial Reynolds number, where the predicted data are slightly higher than the experimental data. In the case of stationary outer cylinder, lower value for Nusselt number was predicted than that of the experimental data. The difference between the experimental and theoretical data diminishes with the increase

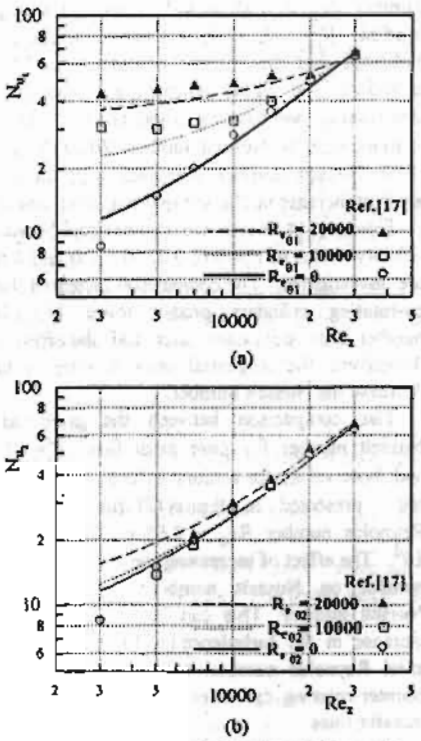

Figure (9) Nusselt number versus axial Reynolds number for different rotational Reynolds numbers at z/D_h = 60 for: a) Inner cylinder rotating.
b) Outer cylinder rotating.